



available at www.sciencedirect.com



journal homepage: www.elsevier.com/locate/jhydrol



Discharge of nitrate-containing groundwater into a coastal marine environment

Martin Søgaard Andersen ^{a,*}, Ludovic Baron ^b, Jacob Gudbjerg ^c,
Jesper Gregersen ^d, Dominique Chapellier ^b, Rasmus Jakobsen ^a,
Dieke Postma ^a

^a Institute of Environment and Resources DTU, Technical University of Denmark, Denmark

^b Institut de Géophysique, University of Lausanne, Switzerland

^c DHI Water and Environment, Denmark

^d Ribe County, Denmark

Received 22 March 2006; received in revised form 20 December 2006; accepted 21 December 2006

KEYWORDS

Submarine ground
water
discharge;
Geophysics;
Nitrate;
Coastal zone;
Modeling

Summary The discharge of nitrate-containing fresh groundwater from a sandy coastal aquifer and into the adjacent shallow marine environment was investigated near Esbjerg at the northern end of the Wadden Sea in Denmark. The geological structure of the coastal site was determined from drilling data and geoelectrical methods such as multi-electrode profiling (MEP). The distribution of shoreface sediment containing freshwater was mapped using MEP, underwater multi-electrode profiling (UMEP) and the electrical conductivity measured on pore waters. Freshwater discharge fluxes were measured using seepage meters and estimated from observed head gradients and measured hydraulic conductivities in the aquifer sediments. The nitrate distribution in the coastal sediments was obtained from water samples. A groundwater flow model was established to quantify the groundwater flow and travel times, and the distribution of freshwater discharge along the coastline. Results show that on the watershed scale the fresh groundwater discharge is controlled by sand filled buried channels that connect the aquifer with the shoreface sediments. The freshwater discharge along the coastline is at this scale probably best estimated by the groundwater flow model. However, at a more detailed scale the distribution of freshwater discharge in the intertidal zone is controlled by small scale geological heterogeneity and models are unable to predict what happens at a small scale on the beach and offshore. For that purpose UMEP, seepage meters, pore water sampling and local hydraulic gradients are more useful. These measurements indicate that the freshwater discharge occurs in distinct zones and that the highest discharge is near the high tide

* Corresponding author. Address: School of Civil and Environmental Engineering, University of New South Wales, Water Research Laboratory, King Street, Manly Vale, 2093 NSW, Australia. Tel.: +61 2 9949 4488x224 (office)/0406 937 178 (mobile); fax: +61 2 9949 4188. E-mail address: m.andersen@wrl.unsw.edu.au (M.S. Andersen).

line, decreasing rapidly in a seaward direction. Nitrate is abundant in the shallow groundwater of the coastal aquifer and is also present in the discharging fresh groundwater at certain patches along the coast. However, on average very little nitrate is observed in the freshwater discharging at the coast. The maximum travel time of groundwater through the aquifer until it discharges at the coast is 100 years and since nitrate leaching from soils has only taken place during the last 40–50 years, part of the fresh groundwater discharging at the coast must be free of nitrate.

© 2007 Elsevier B.V. All rights reserved.

Introduction

In recent years increasing groundwater nitrate concentrations have been reported from aquifers beneath farmed lands especially in Europe and in Northern America (Postma et al., 1991; Spalding and Exner, 1993; Howarth et al., 1996; Iversen et al., 1998). In those cases where the nitrate is not degraded within the aquifer it may appear in groundwater discharge zones in rivers (McMahon and Böhlke, 1996; Puckett et al., 2002), lakes (Loeb and Goldman, 1979; Brock et al., 1982), and coastal marine water bodies (Valiela et al., 1978; Johannes, 1980; Capone and Bautista, 1985; Lewis, 1987; Giblin and Gaines, 1990; Valiela et al., 1992; Matson, 1993; Staver and Brinsfield, 1996; Portnoy et al., 1998). Groundwater may contain nitrate at a millimolar level (1–2 mM) which is very high compared to typical levels within the receiving surface water bodies (Valiela et al., 1978; Johannes and Hearn, 1985; Valiela et al., 1990; Giblin and Gaines, 1990). For example, annual averaged dissolved inorganic N concentrations of Danish estuaries for the years 1989–1995 were in the range of 0–0.2 mM, with an annual median of 0.026 mM (Conley et al., 2000). In particular there has been a growing awareness that submarine groundwater discharge may play an important role as a source of nutrients to coastal waters (Johannes, 1980; Lewis, 1987; Valiela et al., 1990; Lapointe et al., 1990; Matson, 1993; Moore, 1996; Corbett et al., 1999; Rutkowski et al., 1999; Taniguchi et al., 2002; Burnett et al., 2003). Because the primary production of coastal marine environments is often limited by nitrate (Ryther and Dunstan, 1971; Howarth, 1988; Conley et al., 2000; Slomp and Capellen, 2004), groundwater derived nitrate may contribute significantly to eutrophication (Capone and Bautista, 1985; Valiela et al., 1992; Paerl, 1997) and harmful algal blooms (Paerl, 1997).

The mode of fresh groundwater discharge, whether it is occurring at discrete vents (Zektzer et al., 1973; Valiela et al., 1990; Swarzenski et al., 2001) or in a dispersed zone (Bokuniewicz, 2001; Bokuniewicz et al., 2003) as well as the factors affecting the discharge of groundwater nitrate to coastal water bodies remains poorly understood (Valiela et al., 1990; Paerl, 1997; Moore, 1999; Conley et al., 2000; Burnett et al., 2002; Bokuniewicz et al., 2003; Burnett et al., 2003; Schlüter et al., 2004; Jickells, 2005).

Evaluating the discharge of groundwater nitrate into the coastal marine environment poses a complex and interdisciplinary problem. It requires the elucidation of various aspects such as; the hydrogeology and spatial distribution of freshwater and seawater in the shoreface sediments, the flux of freshwater passing through the shoreface into the

marine environment, the accompanying flux of nitrate into the marine environment and finally the degradation of nitrate in both aquifer and marine sediments.

In this paper we will demonstrate how various methods can be combined into an integrated assessment of the discharge of groundwater nitrate into the marine environment. The nitrate degradation processes taking place in the shoreface sediments and in the aquifer will be discussed elsewhere (Andersen et al., in preparation).

Our field site is located near Esbjerg, Denmark, at the northern end of the Wadden Sea (Fig. 1b). Here the groundwater in a sandy coastal aquifer is contaminated with nitrate in concentrations up to about 1 mmol NO₃⁻/L (mM) derived from agricultural activities (Fig. 1a). The aquifer discharges westward into the sea forming a suitable study site for our investigations.

Materials and methods

Geophysical surveying

Underwater multi-electrode profiling (UMEP) was used to map the distribution of seafloor sediments saturated with either freshwater or seawater. The UMEP method, inspired by the work by Lagabrielle and Teilhaud (1981) and Lagabrielle (1983), is based on the direct-current resistivity method. An array of electrodes was towed along the seafloor after a boat. Two electrodes (A,B) 10 m apart on the array emitted current pulses of up to 10 A with durations of 1–2 s. The resulting potential field is measured by eight potential electrodes arranged with one electrode 50 m away from the B electrode on one side and the remaining seven electrodes on the opposite side with logarithmical increasing distances to the A electrode. The position of the boat was continuously recorded by GPS and the depth measured by sonar. Simultaneously seawater conductivity and temperature were measured. The inversion of the UMEP data was done by a code developed specifically for the measuring array. The data was interpreted assuming a three-layer model: surface seawater constitutes the first layer with the resistivity fixed by the conductivity probe measurements; a surface sediment layer of varying depth and resistivity; and finally an infinitely deep layer of varying resistivity. Lateral continuity of the inverted dataset along the survey lines was attained by using the inverted results at one measuring position as initial guess for the following position. The combined probable uncertainty on the UMEP data, combining the data uncertainty and the inversion uncertainty, is around 10%. However, this is probably of minor importance considering the heterogeneity seen in the direct measurements, implying that only larger patches of freshwater discharge, on the

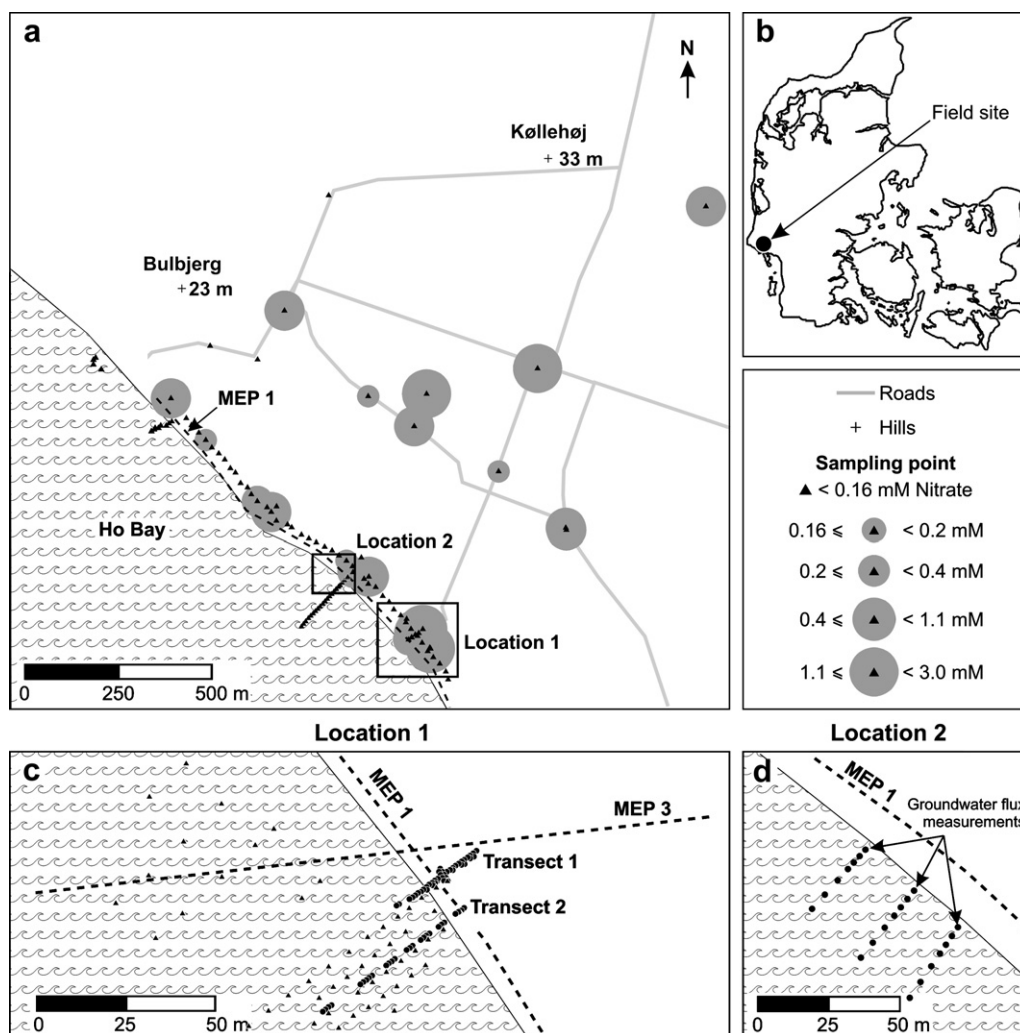


Figure 1 (a) Nitrate distribution in the shallow groundwater of the studied catchment in mmol/L. Triangles are sampling locations; (b) Location of the Ho Bay field site in Denmark; (c) Location 1; (d) Location 2. In (c) and (d) dashed lines indicate MEP profile lines, circles are sampling points in Transects 1 and 2, and the triangles indicate sampling by the 0.01 m o.d. steel pipes.

order of tens of meters, will show up. The method is, however, very sensitive to thin layers of freshwater, so layers of about 0.5–1 m in thickness will be detected if the lateral extent is large enough.

Subsurface geology and the distribution of fresh and salt-water in the subsurface of the beach and intertidal zone were mapped by multi-electrode profiling (MEP). The method utilizes an array of steel electrodes inserted into the ground with an electrode spacing varying from 1 to 5 m depending on the targeted measuring depth (Dahlin, 1996). An ABEM SAS 300C instrument and an IRIS SYSCAL 48 instrument were used to control the excitation of the current electrodes and the measurements at the potential electrodes. The measured apparent resistivities were inverted using the RES2DINV software (Loke and Barker, 1996) to produce a calculated resistivity distribution of the subsurface. Generally five iterations were applied to the data to obtain a root mean square error less than 7%. To get an estimate of the uncertainty we have compared the MEP results with two lithological well-logs near two MEP survey lines. For a sand/clay interface 30 m below the surface, the MEP interpretations were 1 and 5 m off,

respectively. Because of the inherent exponential decrease in resolution with depth for the MEP method, the uncertainty in locating a geological boundary should decrease for shallower depths. However, as for the UMEP method 3D variations in the geology could introduce much larger uncertainty when interpreting the data in 2D.

Pore water sampling and hydrogeological surveys

Pore water samples were extracted from beach and intertidal zone sediments by a drive point technique (triangles in Fig. 1a and c). Steel pipes (0.01 m o.d.) with a 5 cm screened tip were driven into the sediment by a battery powered percussion drill. The pore water sample was retrieved by suction using a 60 mL syringe and a three-way valve attached to the top of the pipe. Three pipe volumes were purged before sampling. The electrical conductivity (σ_w) of the pore water was measured with a WTW Tetracon 96 conductivity probe connected to a WTW LF-196 conductivity meter. The nitrate concentration was estimated in the field using analytical test strips (Merckoquant[®] no. 1.10020.0001, range 10–500 mg NO₃⁻/L).

Two transects from the upper beach and out into the intertidal zone (Fig. 1c) were equipped with permanent piezometers. These were constructed of either 25 or 32 mm o.d. PE pipes and fitted with a 0.12 m screen of 50 μm PE mesh. The piezometers were installed to depths of up to 10 m using a Geoprobe 54 DT drill-rig and 2 $\frac{1}{8}$ in. steel pipes with a disposable PE tip.

Groundwater samples were extracted from the piezometers using a gas-lift technique operating on nitrogen gas (Andersen et al., 2005). The piezometers were flushed three times and then sampled. Samples for nitrate were filtered through a 0.2 μm Satorius Minisart filter, frozen, and later analysed by ion chromatography (HPLC) using a Vydac 30211C column.

The submarine groundwater discharge (SGD) in the intertidal zone was measured by submerged seepage meters (Lee, 1977). The seepage meters were constructed from the top (0.14 m) of an oil barrel (0.6 m i.d.). An outlet on the top was fitted with a plastic hose and connected to a 4 L plastic collection bag, equipped with a valve. The seepage meter was inserted about 0.1 m into the sediment and rested for about 20 min to reach flow equilibrium. Several measurements were made at each position covering 1–2 tidal cycles. Three seepage meters were employed simultaneously in three parallel transect lines each with seven positions covering about 30 m out into the intertidal zone (Fig. 1d). The measurements were done during 11 days in September 2002. The electrical conductivity of the collected water was measured to determine the proportions of freshwater and seawater. Depending on the seepage rate, 1–5 h were required to flush the seawater initially trapped in the seepage meter at insertion. Flushing of the initial seawater was assumed when the electrical conductivity of successive collected volumes of water were constant. The discharge flux was calculated from the sample volume, the collection time and the cross-sectional area of the seepage meter (0.25 m²).

The electrical conductivity measured in the collected water and in the bay surface seawater was used to estimate the submarine fresh groundwater discharge component (q_{SFGD}) of the total submarine groundwater discharge flux (q_{SGD}) according to

$$q_{\text{SFGD}} = q_{\text{SGD}} \cdot \left[1 - \frac{(\sigma_x - \sigma_{\text{fresh}})}{(\sigma_{\text{sea}} - \sigma_{\text{fresh}})} \right] \quad (1)$$

where σ_{fresh} , σ_{sea} and σ_x is the electrical conductivity of fresh groundwater, seawater and the collected water of a particular flux measurement, respectively. In the equation σ_{sea} is the average of σ_{sea} measured in the bay during the experiment. During the tidal cycle σ_{sea} fluctuates up to 3080 $\mu\text{S}/\text{cm}$ which is large compared to the freshwater σ_{fresh} of only 350 $\mu\text{S}/\text{cm}$. This implies that the estimation of the fraction of freshwater is difficult for small fractions of freshwater. However, this is of minor significance as the difference in freshwater flux between a value calculated from the mean σ_{sea} and the $\sigma_{\text{sea-min}}$ and $\sigma_{\text{sea-max}}$ never exceeded $5.2 \times 10^{-8} \text{ m}^3/\text{m}^2/\text{s}$. The fresh water flux per meter coastline was obtained by integrating seaward along the transect lines assuming a constant discharge between the midway point of the previous and following measuring sta-

tion. For the first station the distance to the high tide line (ca. 3 m) were used instead and for the last station a distance seawards was set equal to the distance to the previous midway point.

The hydraulic conductivity in the coastal zone sediments was obtained from slugtests in the two piezometer transects at Location 1 (Fig. 1c), using the vacuum method of Andersen (2001) and analysed by the Hvorslev method (Hvorslev, 1951). The difference between the initial head and the head created by the vacuum was typically in the order 1–1 $\frac{1}{2}$ m. The recovery of the water level was monitored with a small generic pressure transducer (Drück) and a single channel 12 bit Pico-logger set for logging every 0.5 or 1 s. For wells screened in low-permeable layers with a hydraulic conductivity (K) less than $1 \times 10^{-6} \text{ m/s}$ the vacuum method was not used. Instead the water level in the well was lowered by 1–2 m and the recovery of the water level was monitored manually with a dip meter.

Numerical modeling of groundwater flow, travel times and nitrate leaching

Groundwater flow and travel times in the catchment area were modeled with the MIKE-SHE code (Graham and Butts, 2005). Groundwater recharge and the nitrate leaching through the root zone of the agricultural areas were calculated by the deterministic one-dimensional agro-ecological DAISY code (Abrahamsen and Hansen, 2000). The DAISY code calculates recharge and nitrate leaching through the root zone based on daily atmospheric observations (precipitation, temperature and solar radiation), soil type and land-use (crop types and fertilizer application). The code considers both physical and biogeochemical processes (including plant nitrogen uptake, nitrogen mineralization, nitrification and denitrification) in the root zone related to the crop production (Abrahamsen and Hansen, 2000). Using DAISY-GIS (DHI, 2004) the catchment was divided into polygons representing different combination of land-use and soil types for which a 1D DAISY simulation were performed to obtain spatially distributed estimates of recharge and nitrate leaching for the catchment over a 13 year period from 1989 to 2001.

Results

A geological model of the catchment area is shown in Fig. 2. The model is based on results of MEP surveys in combination with records from existing boreholes, outcrops and hand drillings. The aquifer consists of sandy sediments of Quaternary and Neogene age deposited in an up to 70 m deep buried valley cut into a thick Neogene clay deposit. Secondary buried channels connect the aquifer to the coast as seen on the southwest edge of Fig. 2. The use of MEP data to identify the bottom clay layer is elaborated upon in the next section.

The catchment is limited by a groundwater divide located about 1400 m from the coast. Since no major streams or rivers are draining the catchment the groundwater must discharge through the shoreface directly into the sea. The groundwater potential lines of Fig. 2 indicate a groundwater flow generally directed towards the coast.

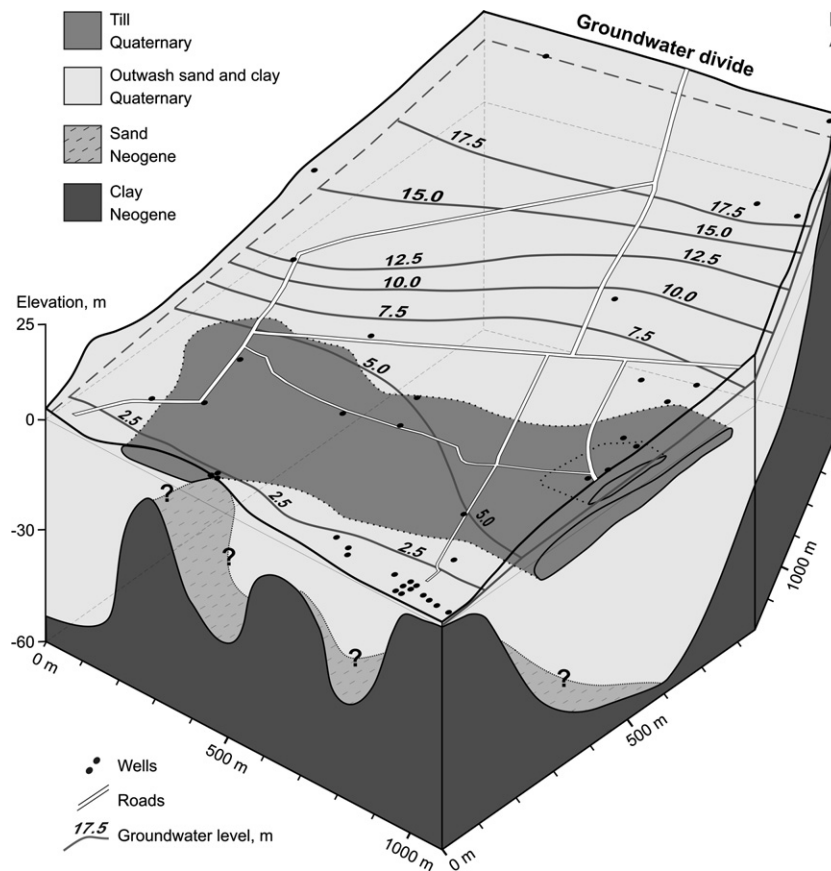


Figure 2 Geological and hydrogeological block model of the catchment. Note vertical scale is exaggerated.

Distribution of fresh- and saline groundwater at the coast mapped by geophysics

Fig. 3a shows the inverted bulk resistivity (ρ_b) distribution in a depth profile along the coast (MEP 1 in Fig. 1a). The ρ_b ranges between $1 \Omega \text{ m}$ and $500 \Omega \text{ m}$. The zones of higher resistivity ($\rho_b > 30 \Omega \text{ m}$), generally found in the upper part of the profile, uniquely identify sandy sediments saturated with freshwater. The low resistivity zones deeper in the profile either represent sediments saturated with saline or brackish groundwater, or Neogene clay. At several locations along the MEP profile a low resistivity was found to correlate with Neogene clay present in outcrops or in drillings (not shown). The top of the clay layer in Fig. 2 was therefore interpreted to be positioned at the $30 \Omega \text{ m}$ contour for the whole profile (thick black line in the MEP profile of Fig. 3a).

The results of the offshore UMEP survey are shown in Fig. 3b. The grey scale represents the inverted bulk resistivity (ρ_b) of the second layer (at approx. 2–3 m below the sea surface), and ranges between a few $\Omega \text{ m}$ and $90 \Omega \text{ m}$. The inverted thickness of this second layer varies between 2 m and 40 m, although for the larger thicknesses the estimate becomes very uncertain. The bulk resistivity of the third layer is generally below $30 \Omega \text{ m}$ and reflects the presence of either clay layers or sandy sediments saturated with brackish or saline groundwater. The UMEP resistivity distribution (Fig. 3b) shows two distinct zones of high resistivity

($\rho_b > 30 \Omega \text{ m}$ or $\sigma_w < 1300 \mu\text{S/cm}$) along the coast, indicating sediments saturated by freshwater. These zones are potential discharge areas for fresh groundwater. For both zones the resistivity decreases in a seaward direction indicating that the UMEP survey probably has captured the seaward extent of freshwater discharge.

Several short MEP profiles were measured in the intertidal zone perpendicular to the coastline. Fig. 4 shows MEP 3 located near the southern high resistivity zone identified by UMEP (Fig. 3b) and was conducted with an electrode spacing of 5 m and a penetration depth of about 30 m. The inverted bulk resistivity measured in the profiles varies between a few $\Omega \text{ m}$ at the seaward end, to more than $100 \Omega \text{ m}$ at the landward end and encompasses the interface between the fresh and saline groundwater. Fresh to brackish groundwater extends about 60 m into the intertidal zone below a zone of low resistivity seawater several meters thick. In Fig. 4 the distal salt-/freshwater interface at about 40 m is almost vertical implying an upward flow of fresh groundwater on the landward side. This is assuming a quasi-steady state where no major horizontal movement of the salt-/freshwater interface takes place. In the upper part of the intertidal and supratidal zones there are plumes of low to intermediate resistivity ($10\text{--}50 \Omega \text{ m}$) overlying the fresh groundwater. These appear to be related to the flooding with seawater during high tide and storms (see Discussion).

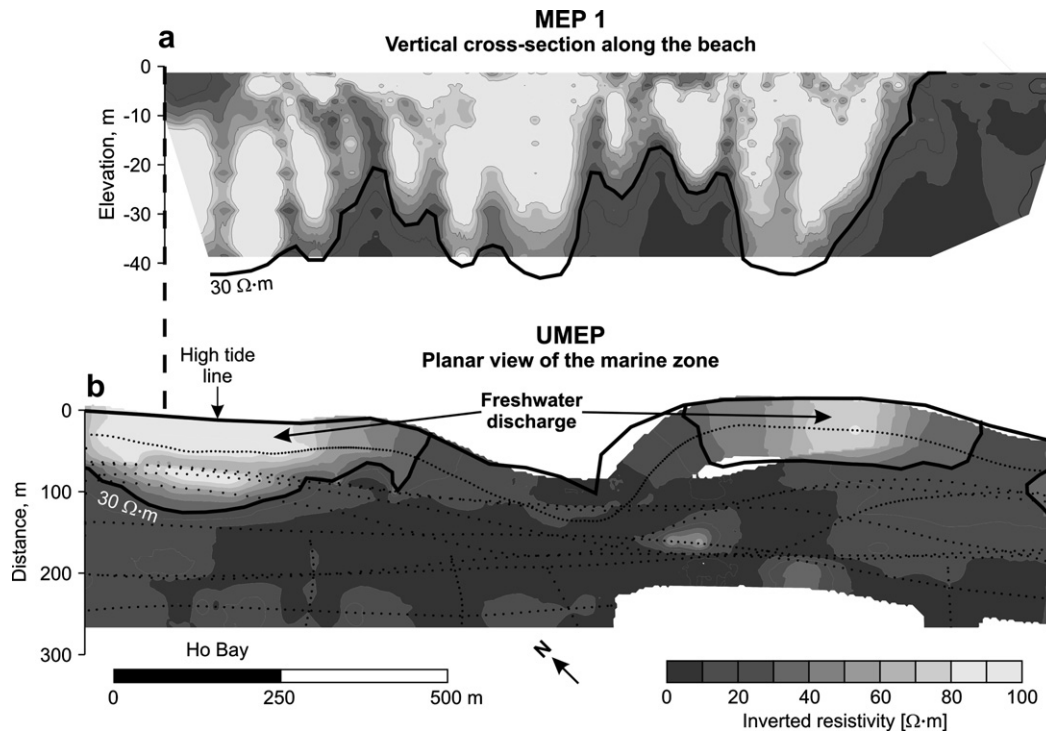


Figure 3 Geophysical surveys in the coastal zone. (a) Vertical section along the beach showing the inverted bulk resistivity ($\Omega\text{ m}$) of the MEP 1 profile (see Fig. 1a for location). The solid black line denotes $\rho_b > 30\ \Omega\text{ m}$ and represents the interpreted interface between the freshwater saturated sand and the clay or seawater (note: the vertical scale of the MEP is exaggerated). (b) Planar view of the offshore UMEP survey traces (dotted lines) with contoured bulk resistivities ($\Omega\text{ m}$) from second layer of the inverted UMEP-data. High resistivities ($\rho_b > 30\ \Omega\text{ m}$) are confined by the solid black line and represents freshwater discharge zones.

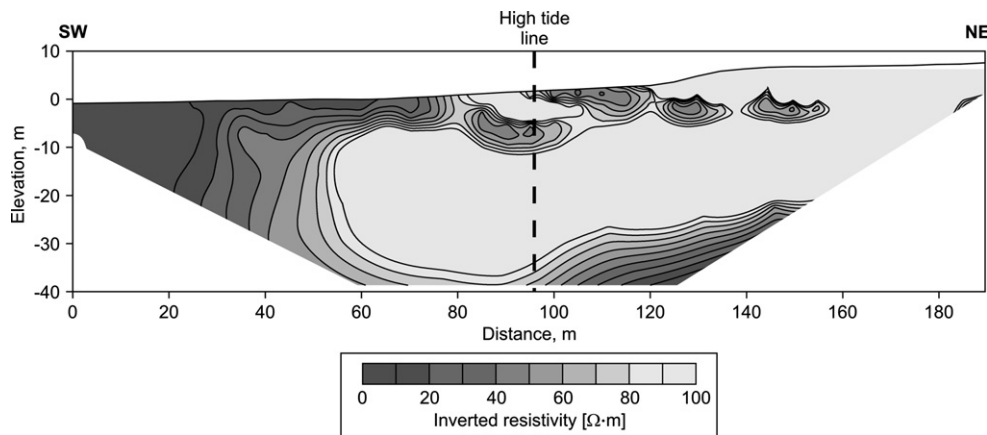


Figure 4 Vertical section of the inverted bulk resistivity ($\Omega\text{ m}$) measured in the intertidal zone by MEP showing the seawater–freshwater interface along transect line MEP 3 at Location 1 (Fig. 1c). A high resistivity indicates the presence of freshwater.

Pore water resistivity of the intertidal zone sediments

The electrical conductivity (σ_w) was measured in pore water samples from different depths in the intertidal zone to obtain a more detailed description of the distribution of seawater and freshwater in the upper sediments (<1.2 m). The measured σ_w of the pore water varied from 340 to 40,000 $\mu\text{S}/\text{cm}$, covering the range from pure fresh groundwater to surface seawater of the bay.

The pore water σ_w was recalculated to bulk resistivity for comparison with the bulk resistivities obtained by the geophysical methods. First the measured electrical conductivity is converted from the reference temperature of $T = 25\text{ }^\circ\text{C}$ to the ambient groundwater temperature of $T = 10\text{ }^\circ\text{C}$ by using the Arps (1953) conversion equation for NaCl-brines as given by Worthington et al. (1990):

$$\sigma_{w,10^\circ} = \sigma_{w,25^\circ} \cdot \frac{(T_{10^\circ} + 21.5)}{(T_{25^\circ} + 21.5)} \tag{2}$$

The pore water resistivity (ρ_w) is calculated from $\rho_w = 1/\sigma_w$ and relates to the bulk resistivity (ρ_b) according to Archie's law (Telford et al., 1990):

$$\rho_b = a \cdot \phi^{-m} \cdot \rho_w \quad \text{or} \quad F = \rho_b / \rho_w \quad (3)$$

ϕ is the porosity, a and m are empirical values and F is the formation resistivity factor. Eq. (3) does not account for the conductive contribution by clay particles present in the sediment (Urish, 1981; Bai, 1989). However, for sandy sediments F appears to be relatively constant as long as the pore water resistivity is below 20–30 Ω m (i.e. a pore water conductivity (σ_w) higher than 330–500 $\mu\text{S}/\text{cm}$) (Bai, 1989). This condition is satisfied for most pore water conductivities measured in the intertidal zone, except for a few low values in the range of 340–500 $\mu\text{S}/\text{cm}$. The porosity was estimated to 0.4 using core samples. Lacking actual determinations of a and m for the sediments at the field site, average values of a and m for fluvial deposited sands from the Danish Forest and Nature Agency (1987) were used. Archie's law is then expressed as

$$\rho_b = 1.26 \cdot (0.4)^{-1.2} \cdot \rho_w \Rightarrow F \approx 4 \quad (4)$$

Bai (1989) reported a formation factor of about 4 (range: 3–5) for quaternary and tertiary sandy sediments from different sedimentary environments in Denmark. In any case the observed variation in the pore water conductivity, due to the variation in salt content, by far outranges the uncertainty in the formation factor.

Fig. 5 shows the results of the pore water σ_w -data at 0.3 m depth (dots representing sampling sites) converted to bulk resistivities (ρ_b) for Location 1 (see Fig. 1c). The

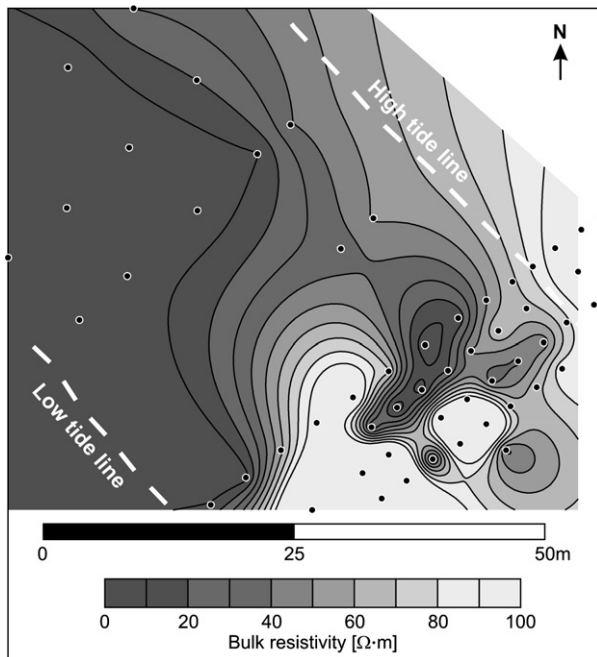


Figure 5 Planar view of the calculated bulk resistivity (Ω m) in the pore water based on electrical conductivity measurements in the intertidal zone at Location 1 (Fig. 1a and c), at 0.3 m below the sediment surface (see Appendix A, Fig. A.1 for the distribution at 0.6, 0.9 and 1.2 m below the sediment surface).

area is on the northern margin of the southern freshwater discharge zone found by UMEP (Fig. 3b). The bulk resistivity in Fig. 5 shows large spatial variations. In the uppermost layer (0.3 m, Fig. 5) the ρ_b is generally low, down to 1.5 Ω m, due to flooding of the sediment surface with seawater at high tide. With increasing depth the resistivity increases as freshwater becomes dominant. There is also a lateral variation at the depths of 0.3, 0.6 and 0.9 m with more seawater towards northwest and more freshwater towards the southeast and the shore. An isolated body of brackish water was found down to a depth 1.2 m (see Appendix A, Fig. A.1, for results at 0.6, 0.9 and 1.2 m).

A comparison with UMEP data for the same zone shows that the UMEP data has a much coarser resolution because the UMEP array averages over a larger area (lowermost chart in Appendix A, Fig. A.1). However, there is a general agreement with pore water σ_w -measurements as both methods indicate the presence of more saline water towards the northwest and more freshwater towards the southeast.

Hydraulic conductivity

The hydraulic conductivity was measured by slugtests in the two piezometer transects of Location 1 (Fig. 1c) and ranged from 3.9×10^{-7} m/s to 1.1×10^{-4} m/s (average of 2.3×10^{-5} m/s, std. dev. = $\pm 1.26 \times 10^{-5}$ m/s). These values correspond to fine grained sand containing small lenses of silt and clay. No spatial trends in the distribution of the hydraulic conductivity in the two transects could be discerned (Mikkelsen, 2004). Pumping tests in inland wells showed transmissivity values of around $0.5-1 \times 10^{-3}$ m²/s, corresponding to a hydraulic conductivity of approximately 3×10^{-5} m/s for an aquifer with an average thickness of 20 m (Ribe County, 2003).

Hydraulic head distribution

The hydraulic head was measured in the two transects at Location 1 (Fig. 1c) at both high and low tide. Generally the hydraulic head decreases in a seaward direction. In Transect 1, covering mainly the supratidal zone, the change in hydraulic head from low tide to high tide is small (see Appendix A, Fig. A.2). At the seaward end the hydraulic head increases about 0.3 m from low to high tide, whereas at the landward end the increase is about 0.1 m. The groundwater flow direction, inferred from the contours of equal hydraulic head, only changes slightly with a more upward direction at the seaward end of Transect 1 at high tide. Transect 2 is mainly situated in the intertidal zone and the changes in hydraulic head from low to high tide are larger (Fig. 6a and b). At the landward end of Transect 2 the hydraulic head increases about 0.2 m from low to high tide. At the seaward end the increase in hydraulic head is more than 1 m, equivalent to the hydrostatic pressure of the overlying seawater at high tide. At low tide the groundwater seems to be flowing horizontally seaward at a high rate, as indicated by the large hydraulic gradient (Fig. 6a). Some of this groundwater must be discharging along the entire extent of the intertidal zone, which is supported by the observation of a broad seepage face at low tide. With the rising tide the flow direction changes to be mainly upward while the associated discharge must de-

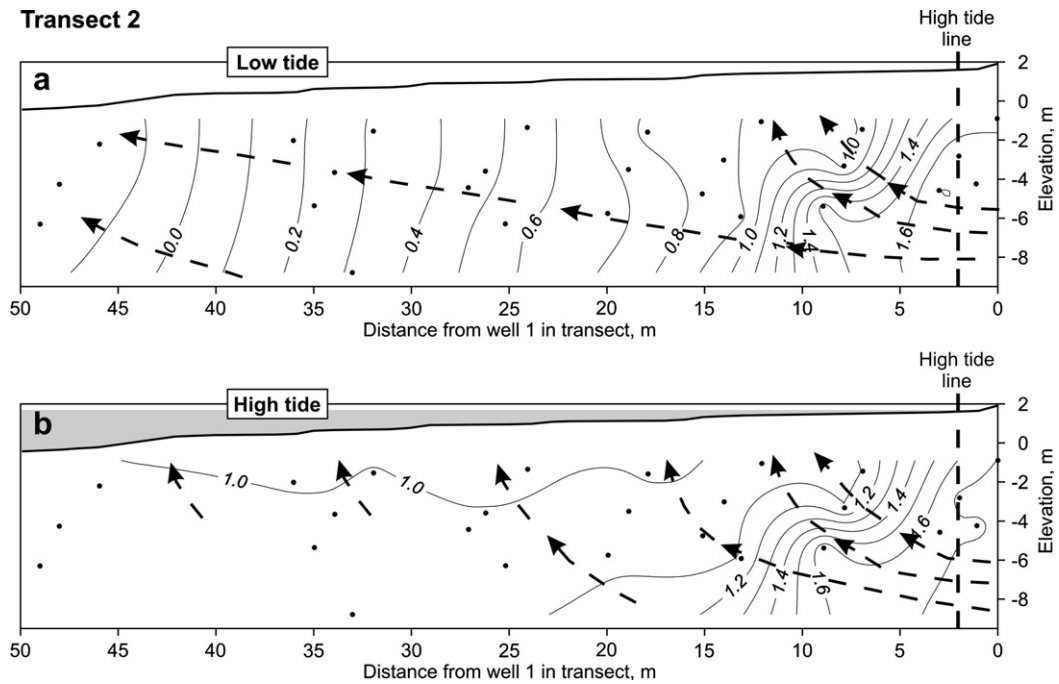


Figure 6 Hydraulic head (m) distribution in piezometers along Transect 2 at Location 1 (Fig. 1c) and inferred flow paths: (a) Transect 2 at low tide; (b) Transect 2 at high tide. The low tide line is beyond the seaward extent of the transect (see also Appendix A, Fig. A.2 for Transect 1).

crease as indicated by the low hydraulic gradient (Fig. 6b). Similar patterns of tide dependent groundwater discharge were found by Staver and Brinsfield (1996) and Portnoy et al. (1998). The steep hydraulic gradient observed around 5–15 m in Transect 2 (Fig. 6a and b) probably reflects a local zone of enhanced upward flow since there are no significant variations in the hydraulic conductivity across this zone. No surface seepage was observed immediately above,

so this groundwater must discharge seawards possibly through coarse grained sediments in the upper beach.

Submarine fresh groundwater discharge (SFGD)

The submarine groundwater discharge flux (q_{SGD}) was measured in three parallel transects in the intertidal zone (Location 2 in Fig. 1a and d and Fig. 7a). At each station 2–4

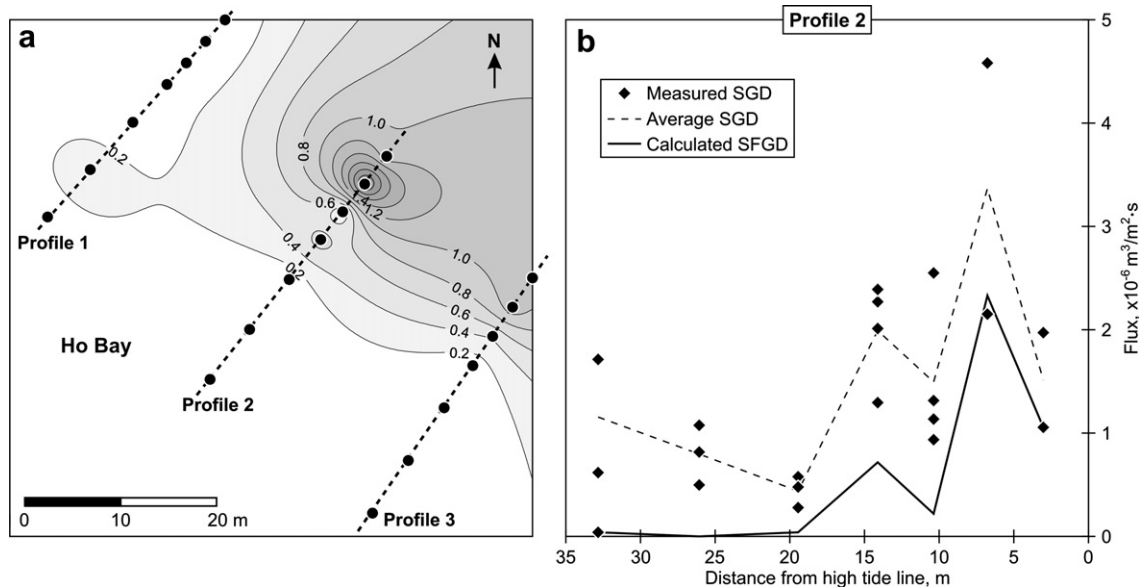


Figure 7 Submarine groundwater discharge (SGD) and the estimated submarine fresh groundwater discharge (SFGD) measured by seepage meters at Location 2 (Fig. 1d). (a) Contoured SFGD $\cdot 10^{-6} \text{ m}^3/\text{m}^2 \text{ s}$ in the intertidal zone. (b) Measured SGD and calculated SFGD in $\text{m}^3/\text{m}^2 \text{ s}$ for Profile 2. The integrated discharge flux is $1.8 \times 10^{-5} \text{ m}^3/\text{s}$ per meter coastline (see also Appendix A, Fig. A.3 for Profiles 1 and 3).

measurements were done. The results from Profile 2 are plotted in Fig. 7b (for Profiles 1 and 3 see Appendix A, Fig. A.3). The fluxes varied considerably over time at a given station and the variations do not correlate with the tidal cycle, in agreement with Giblin and Gaines (1990) and Cable et al. (1997b), but contrary to what has been reported elsewhere (Lee, 1977; Lewis, 1987; Robinson et al., 1998; Taniguchi et al., 2003; Taniguchi and Iwakawa, 2004). There are also major variations in measured discharge fluxes from one transect to the next even though they are located only 20 m apart. However, both Profiles 2 and 3 yield the highest discharge flux at the landward end of the transect.

Seepage meters may produce erroneous discharge estimates in areas with high waves or surface water flow velocities (Lee and Cherry, 1978; Libelo and MacIntyre, 1994; Duff et al., 2000; Shinn et al., 2002; Murdoch and Kelly, 2003; Taniguchi et al., 2003). Such phenomena can produce an additional artificial flux by introducing seawater via the sediment into the seepage meter (Libelo and MacIntyre, 1994; Shinn et al., 2002; Murdoch and Kelly, 2003). Waves and along shore current of up to 0.8–1.0 m/s (caused by tides moving water in and out of the bay) did vary throughout the 11 days of the measuring campaign. These effects were not recorded accurately enough to enable a correlation to the measured rates. It may therefore not be possible to obtain reliable estimates of q_{SGD} (seawater + freshwater) in the intertidal zone. However, the freshwater component of the discharge flux (q_{SFGD}) can be estimated by using the electrical conductivity of the collected water (see Eq. (1)) since wave action will only introduce extra seawater and not freshwater. When the discharge fluxes are corrected for the seawater contribution in order to obtain q_{SFGD} , they reduce to very low values for most of Profile 1 and at the seaward end of Profiles 2 and 3 (Fig. 7a and Appendix A, Fig. A.3). In the landward 10–15 m of the intertidal zone the q_{SFGD} for Profiles 2 and 3 is $0.5\text{--}2 \times 10^{-6} \text{ m}^3/\text{m}^2 \text{ s}$, and decreases rapidly seawards. Between the transects the q_{SFGD} varies strongly: In Profile 1 the flux remains below $0.4 \times 10^{-6} \text{ m}^3/\text{m}^2 \text{ s}$ while in Profile 2 it peaks at $2.3 \times 10^{-6} \text{ m}^3/\text{m}^2 \text{ s}$ (Fig. 7a). Integrating the SFGD fluxes along each profile line yield a discharge flux per meter coastline varying from 3.6×10^{-6} to $1.8 \times 10^{-5} \text{ m}^3/\text{m} \text{ s}$.

Distribution of nitrate in the discharging groundwater

Most shallow boreholes in the catchment show a high groundwater nitrate concentration (Fig. 1a). In order to assess to what extent nitrate-containing groundwater is discharging through the shoreline a survey was done where the nitrate content was measured in the shallow groundwater (<1 m) along the high tide line for every 20 m. The results (Fig. 1a) show that the groundwater nitrate concentration was generally below the detection limit of 0.08 mM. However, at a few sites up to 1 mM (62 mg/L) NO_3^- was found (Fig. 1a). Additional pore water measurements downstream from these spots revealed that the nitrate-containing groundwater generally does not extend more than a few meters out into the intertidal zone even though the pore water remains fresh further seaward. Only at one of these spots (Location 1 in Fig. 1c) nitrate was found in the pore water further downstream on the beach.

More detailed investigations at this site show the measured nitrate distribution in the aquifer in the intertidal and supratidal zones (Figs. 8a and 1c). Both transects contain predominantly fresh pore water. In Transect 1 the nitrate concentration varies from 0 to 1.4 mM NO_3^- , but nitrate is only found in the landward end (Fig. 8b), presumably reflecting upwelling NO_3^- -free groundwater in the seaward end. Thus little nitrate appears to reach beyond the high tide line. However, in Transect 2 (Fig. 8c), up to 0.6 mM nitrate was found at depths of at least 5–6 m and more than 35 m seaward into the intertidal zone. This striking difference between the two transects, which are located only 10 m apart, emphasizes the heterogeneous nitrate distribution in the pore waters of the shoreface sediments.

Discussion

Hydrogeology of the coastal aquifer

The collected information on the geological structure in combination with available hydrogeological data was implemented in a groundwater model to characterize the flow conditions in the coastal aquifer and the groundwater discharge along the shoreface. The groundwater model (MIKE-SHE) does not consider density effects. However, the density effect will be insignificant at the catchment scale and the model is not detailed enough to describe the variations in discharge normal to the coastline for which the density effect may play a role.

The geological variation in the groundwater model was distributed according to Fig. 2 with the Tertiary clay layer as an impermeable bottom. The model was discretized horizontally with a mesh of $x = 20 \text{ m}$, $y = 20 \text{ m}$. Vertically the aquifer was divided into 10 layers equally spaced between the soil surface and the aquifer bottom. The upstream boundary, defined by the groundwater divide, is a no-flow boundary. Also the boundaries perpendicular to the coast are no-flow boundaries, as justified by the hydraulic head distribution indicating groundwater flow directed towards the sea (Fig. 2). The model domain extends approximately 400 m into the sea and in this part the top of layer 1 was assigned a constant head of 0.4 m to model the boundary to the sea in accordance with the observed mean bay sea-level, neglecting tidal variations. The hydraulic conductivity of the geological zones was found by automatic calibration of the model in steady state against hydraulic heads measured from 2001 to 2003. Except at the coastal zone where the hydraulic conductivity was kept at an average value of $2.3 \times 10^{-5} \text{ m/s}$ as measured by the slugtests. The calibration procedure led to a reduction in the vertical hydraulic conductivity (K_v) of the geological model near the groundwater divide to obtain an acceptable fit of the observed heads. This reduction in K_v suggests either the existence of low-permeable layers increasing the aquifer anisotropy, or perhaps a perched water table in this zone. Table 1 gives an overview of the model parameters.

The steady state horizontal flow field of layer 4 in the numerical model and three equipotential lines are shown in Fig. 9a. Along the coastline, the flow velocities are highest and converging where the buried channels of sandy sed-

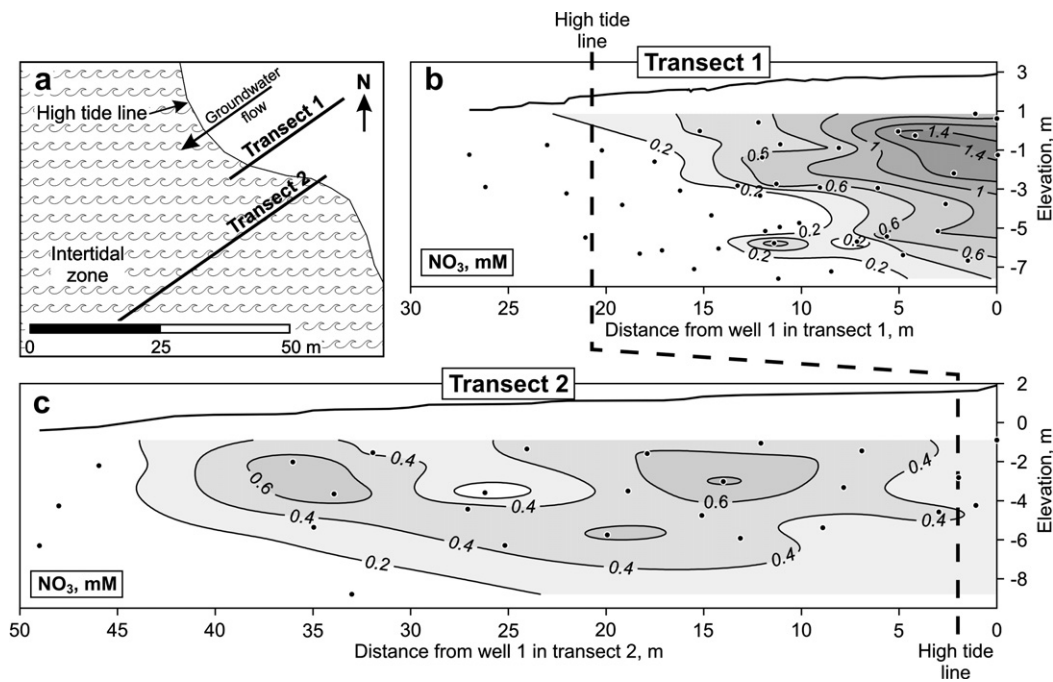


Figure 8 Nitrate distribution (mmol/L) in the beach aquifer and below the intertidal zone in the piezometers along Transects 1 and 2 of Location 1 (Fig. 1c): (a) relative transect locations; (b) Transect 1; (c) Transect 2.

Table 1 Geological properties used in the groundwater model

Zones or geological units	Horizontal hydraulic conductivity (m/s)	Vertical hydraulic conductivity (m/s)	Anisotropy	Porosity	Specific storage
Coast	2.3×10^{-5} ^a	2.3×10^{-6}	10	0.2	1×10^{-5}
Downstream aquifer	2.2×10^{-4} ^b	2.2×10^{-5}	10	0.2	1×10^{-5}
Upstream aquifer	8.0×10^{-5} ^b	8.0×10^{-8}	1000	0.2	1×10^{-5}
Clay lense	4.2×10^{-7} ^b	4.2×10^{-8}	10	0.2	1×10^{-5}

^a Measured.

^b Calibrated.

iments intersect the shoreface and low where the Tertiary clay outcrops (see Fig. 2). In parts of the inland area the bottom of layer 4 is above the water table and consequently there is no horizontal flow component to plot.

In Fig. 9b the vertical flow component is plotted for the boundary between layer 2 and layer 1. In the inland part flow is downwards (negative values) whereas flow is upwards (positive values) in a narrow zone along the coastline where the groundwater discharges into the sea. The seaward extent of the modeled groundwater discharge area in Fig. 9b is a function of the anisotropy of the sand in the beach section. This anisotropy could not be calibrated at the relevant scale from the available data and it was therefore kept arbitrarily fixed at $K_h/K_v = 10$ (Table 1). The flow model gives a steady state total freshwater discharge of $2.4 \times 10^{-2} \text{ m}^3/\text{s}$ (equaling the average modeled groundwater recharge of 396 mm/year).

The results of the hydrogeological investigations and flow modeling illustrate the complexity associated with groundwater discharge through the shoreface. The flow field is heterogeneous due to the geometry of the geological structure. In addition the converging flow lines in the zones of

discharge along the coastline suggest variable flow conditions even at a small scale which is underpinned by our investigations of freshwater discharge at the shoreface and discussed in more detail in the following sections.

Spatial distribution of submarine fresh groundwater

Several methods (UMEP, MEP and pore water samples (σ_w)) were used to locate submarine sediment containing fresh groundwater. The use of different sampling techniques, numerical inversion methodologies and inherent assumptions when converting the results of the three methods to a common parameter, the bulk resistivity ρ_b , warrant a cautious attitude when comparing the results. However, a bulk resistivity above $30 \Omega \text{ m}$ must be considered as a reliable indicator for the presence of freshwater saturated sediments for all three methods. Tronicke et al. (1999) adopted the same value for delineating freshwater saturated sediments in a geophysical survey on the island of Spiekeroog, northern Germany. Using the $30 \Omega \text{ m}$ boundary, a comparison of the MEP and UMEP results of Fig. 3b reveals that

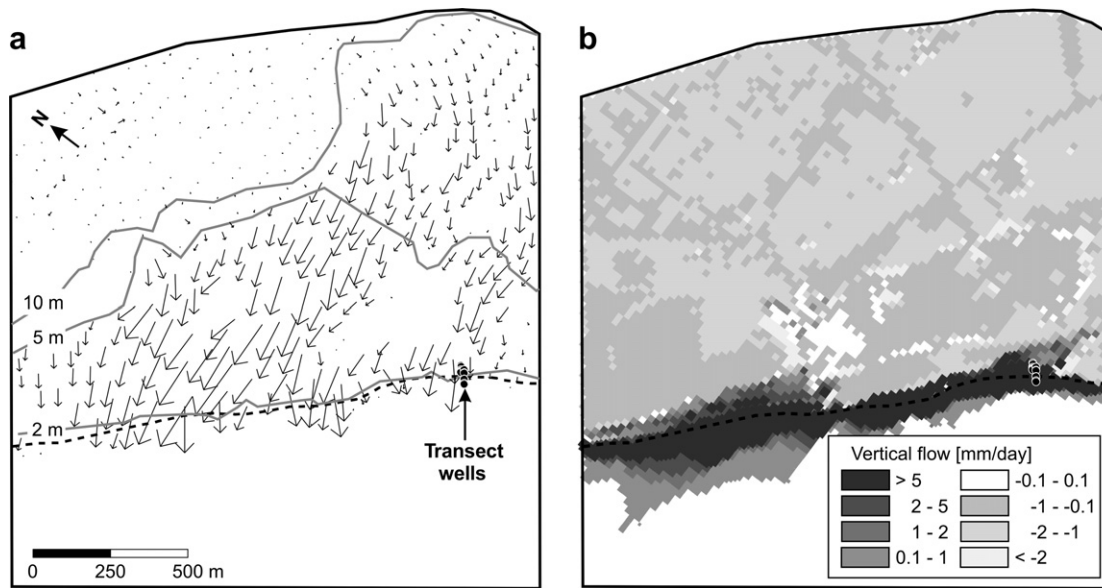


Figure 9 (a) Hydraulic heads and flow velocity and direction of modeled steady state groundwater flow for layer 4 (no velocity vectors are drawn for areas above the water table ("white" areas)); (b) steady state vertical groundwater flow rate (positive upwards) from layer 2 to layer 1 (mm/day). Notice that the plots are rotated relative to north.

the two high resistivity zones found by UMEP correlate well with zones of high resistivity in the coastal MEP 1 profile. In contrast, the high resistivity zones in the coastal MEP 1 profile are not all reflected by zones of high resistivity in the UMEP data. The fresh groundwater discharge appears to converge at the two high resistivity zones according to the UMEP data (Fig. 3b). While the UMEP method gives a good overall picture of the distribution of fresh groundwater in seafloor sediments (Fig. 3b) the method averages over quite large areas and therefore tends to create artificial gradual transitions between fresh- and saltwater saturated sediments. Accordingly small scale spatial variations will not be resolved. This becomes clear from the comparison of the UMEP data with the pore water σ_w -measurements. The central zone of low bulk resistivity in Fig. 5 detected by pore water measurements does not appear in the UMEP survey for the same area (see Appendix A, Fig. A.1). These small scale variations (on the order of meters) are better resolved by the MEP method and better even by direct pore water sampling for σ_w .

Clearly it is not sufficient to map the distribution of freshwater saturated sediments in a vertical section along the beach with MEP. Offshore measurements using techniques such as UMEP are a necessity to resolve the distribution of submarine freshwater in three dimensions and are a first requirement for assessing the freshwater discharge. Vanek and Lee (1991) reached a comparable conclusion for the Laholm Bay in Sweden where onshore investigations were insufficient to capture the complex offshore groundwater discharge. Manheim et al. (2004) and Krantz et al. (2004) also used submarine resistivity surveying to map occurrences of submarine fresh groundwater in several estuaries on the east coast of the US and found a complex distribution of freshwater. Although this distribution probably could not be predicted entirely by the terrestrial geology, there was some indication that it is controlled by submerged paleo-drainage systems (Manheim et al., 2004), much like the bur-

ied channels of this study. In contrast, at the Eckernsörde Bay (Western Baltic Sea) the submarine discharge of fresh groundwater was highly heterogeneous and occurring through distinct pockmarks in the seafloor (Schlüter et al., 2004). The location of these pockmarks could by no means be predicted from shoreface geology (Kaleris et al., 2002).

The two UMEP high resistivity zones of $\rho_b > 30 \Omega \text{ m}$ (Fig. 3b) cover a horizontal area of about 69,800 m². In contrast the corresponding vertical MEP area with $\rho_b > 30 \Omega \text{ m}$, Fig. 3a, is only 27,600 m², yielding a ratio of $\text{Area}_{\text{UMEP}}/\text{Area}_{\text{MEP}} = 2.5$. Most likely the larger UMEP area is due to a horizontal anisotropy in the intertidal and subtidal zone sediments.

Substantial areas outside the high UMEP resistivity zones have intermediate bulk resistivities (1–30 $\Omega \text{ m}$) indicating brackish pore water. These zones could partly be artificial: an averaging tendency of the UMEP method. However, also the ρ_b -values from the MEP profiles done in the intertidal zone (Fig. 4) and the σ_w -data (Fig. 5 and Appendix A, Fig. A.1) show zones with fresh or brackish pore water below sediments saturated with more saline pore water. Similar distributions with salt pore water overlying fresher groundwater have been observed in the intertidal sediments of other beach sites affected by waves and with a tidal range of more than 1 m (Turner and Acworth, 2004; Vandenbohede and Lebbe, 2006; Robinson et al., 2006a). Robinson et al. (2006b) explain the existence of these salt plumes by a circulation of seawater into the beach caused by asymmetric wetting and draining of the beach during the tide cycle in combination with the higher density of the seawater. At our site the salt plumes appear to be unevenly distributed as shown by Fig. 4 with several plumes extending seaward and at varying depths. This heterogeneous distribution is probably partly related to changes in sea-level other than the diurnal tides such as spring/neap tidal cycles and storm events. Undoubtedly geological heterogeneity plays a role too: In some areas the presence of brackish pore waters at depth (>2 m) appears to correlate with the existence of

local clay layers below (Mikkelsen, 2004). Silt/clay lenses present in the intertidal sediments could prevent the salt-water on top of such layers in being flushed by groundwater from below. However, some proportion of the fresh groundwater discharge could emerge through these layers and cause the dispersed discharge of brackish groundwater outside the delineated discharge zones of Fig. 3b, but at a reduced rate.

In contrast the seepage meter data of Fig. 7 shows that the fresh groundwater discharge is predominantly occurring within a narrow zone of the upper 10–15 m of the intertidal zone. Similar narrow discharge zones were found elsewhere. For example, a zone less than 15 wide at the Wye River Estuary, Maryland (Staver and Brinsfield, 1996) and just 1–2 m at Town Cove, Cape Cod (Portnoy et al., 1998).

Fluxes and distribution of freshwater discharge

The discharge of fresh groundwater through the shoreface and into the marine environment can be assessed at different scales by various methods. At the largest scale freshwater discharge rates may be obtained from the water balance on the watershed scale (Oberdorfer et al., 1990; Giblin and Gaines, 1990; Cambareri and Eichner, 1997) or by numerical modeling of groundwater flow (Kaleris et al., 2002; Smith and Nield, 2003; Smith and Zawadzki, 2003; and this study). The modeling approach probably gives a good estimate of the total SFGD from the catchment. For this study site the modeled catchment SFGD only depends on the recharge estimate and the delineation of the catchment area, since no major surface runoff occurs. Here the steady state

groundwater model gave an average freshwater discharge flux per meter coastline of $1.3 \times 10^{-5} \text{ m}^3/\text{s m}$ (Table 2).

The modeled spatial variability of SFGD along the coastline as expressed by Fig. 9a and b is largely controlled by the geological structure in the landward part of the aquifer (Fig. 2). The modeled distribution of the steady state fresh groundwater discharge flux per meter coastline is shown in Fig. 10a. It varies between zero at the clay outcrop to the southeast to about $2.5 \times 10^{-5} \text{ m}^3/\text{s m}$ coastline at the buried valleys. For locations 1 and 2 the model gave a steady state freshwater discharge flux per meter coastline of $1.7 \times 10^{-5} \text{ m}^3/\text{s m}$ and $1.0 \times 10^{-5} \text{ m}^3/\text{s m}$, respectively (Table 2). The seasonal variation in the freshwater discharge was calculated by the model in transient mode (receiving variable recharge from the DAISY-GIS model). In Fig. 10b the modeled transient recharge and discharge for the whole catchment over the 13 year period shows that the freshwater discharge is positively correlated to the winter recharge, but slightly skewed towards spring. In addition Fig. 10b shows how the modeled discharge only varied little over the year compared to the seasonal variation in the recharge due to storage in the aquifer. In Fig. 10a the maximum variation in the freshwater discharge along the coastline is represented by the wet period in March 1995 and the dry period in July 1998. The average minimum dry period discharge only deviates marginally (9%) from the steady state discharge whereas the average maximum wet period discharge is 34% larger than the steady state discharge.

The variations in seaward geology are rarely included in hydrogeological models applied to coastal catchments and they are therefore not likely to give a good picture of the

Table 2 Estimates of fresh groundwater discharge fluxes (q_{SFGD}) per meter coastline (in $\text{m}^3/\text{s m}$) for the field site by various methods and at various scales

Method	Location	Groundwater discharge flux	Comments
Simple water balance	Whole watershed	1.5×10^{-5}	Based on average recharge of 396 mm/year and an average distance to the water divide of 1200 m
Groundwater model	Whole watershed	1.3×10^{-5} ($1.2\text{--}1.8 \times 10^{-5}$)	Total seaward groundwater discharge rate at steady state. Range gives min. and max. discharge from the transient model (March 1995–July 1998)
Groundwater model	Location 1 ^a	1.7×10^{-5} ($1.6\text{--}2.2 \times 10^{-5}$)	Seaward groundwater discharge rate at steady state range gives min. and max. discharge from the transient model (March 1995–July 1998)
Estimated by the gradient method	Location 1 ^a	0.7×10^{-5} ($0.5\text{--}0.9 \times 10^{-5}$)	Based on average hydraulic conductivity of $2.1 \times 10^{-5} \text{ m/s}$, an average gradient of 0.011 and a depth to the bottom of 30 m. Range is min. and max. at tidal stage: (high tide–low tide) Hydraulic gradients measured November 2003 (see electronic attachment 2)
Groundwater model	Location 2 ^a	1.0×10^{-5} ($0.9\text{--}1.4 \times 10^{-5}$)	Seaward groundwater discharge rate at steady state. Range gives min. and max. discharge from the transient model (March 1995–July 1998)
Seepage-meters	Location 2 ^a	1.1×10^{-5} ($0.36\text{--}1.8 \times 10^{-5}$)	Based on an average of three seepage-meter profiles (see Fig. 7a and electronic attachment 3). Range gives max. – min. profile. Measured September 2002

^a See Fig. 1 for location.

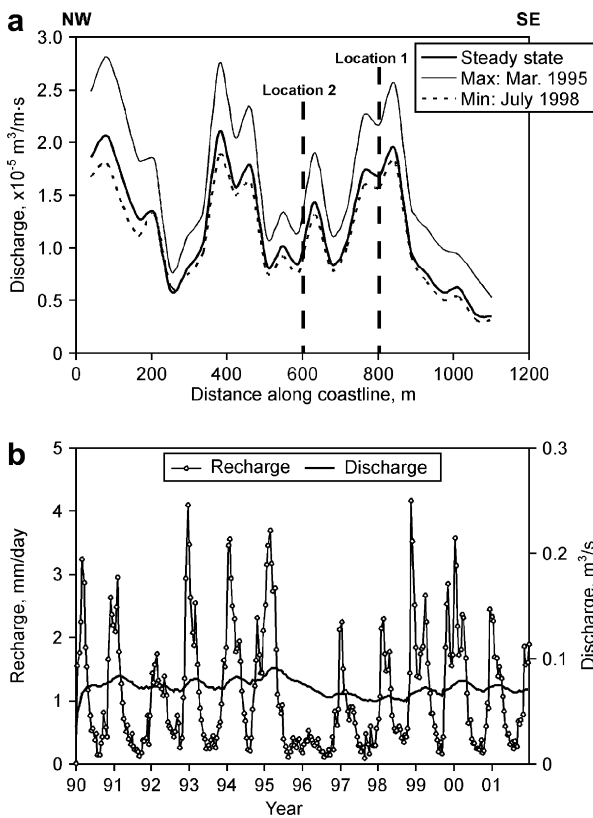


Figure 10 (a) Model calculated discharge of fresh groundwater along the coast (in $\text{m}^3/\text{s m}$ coastline) from the steady state and the transient groundwater model. Only the southern portion of the coastline, equal to the southwestern edge of Fig. 2, is shown. (b) Modeled transient recharge and freshwater discharge (m^3/s) for the whole catchment over the 13 year period from 1989 to 2001.

spatial distribution of the freshwater discharge (Smith and Nield, 2003). In our model, the sub- and intertidal area subject to SFGD, as shown by Fig. 9b, is largely determined by the employed anisotropy (K_h/K_v in Table 1), which was not measured but estimated. The SFGD area of Fig. 9b is thus rather arbitrary.

However, a first estimate of the freshwater discharge flux can be obtained by assuming that the total freshwater discharge of $1.4 \times 10^{-2} \text{ m}^3/\text{s}$ occurs exclusively through the two high resistivity zones of Fig. 3b, with a total area of $69,800 \text{ m}^2$. This gives an average freshwater discharge flux of $2 \times 10^{-7} \text{ m}^3/\text{m}^2 \text{ s}$ (or a pore water velocity of 4.2 cm/day , assuming a porosity of 0.4). The actual pore water discharge velocity may well be smaller considering that a portion of the discharge may be occurring outside the high resistivity zones as more diffuse discharge. Moreover the discharge may be more unevenly distributed than the relatively smooth picture suggested by the UMEP data (Fig. 3b).

At a more detailed scale an estimate of freshwater discharge fluxes can be obtained by the gradient method using the gradients in hydraulic head and measured hydraulic conductivity. For the beach zone such calculations are complicated by the tidal fluctuations causing transient hydraulic gradients and changes in water storage. However, the land-

ward part of Transect 1 (see Appendix A, Fig. A.2) is only marginally affected by the tidal variations. From 0 to 20 m in this transect the head gradients vary from 0.009 to 0.014 over a tidal cycle with an average of 0.011. Using this gradient, together with an average hydraulic conductivity for this zone ($2.1 \times 10^{-5} \text{ m/s}$, $n = 31$) and a depth to the aquifer bottom of 30 m (estimated from the MEP geophysics), gives an average freshwater discharge flux per meter coastline of $0.7 \times 10^{-5} \text{ m}^3/\text{s m}$ (Table 2). In contrast, applying the gradient method further seawards in the intertidal zone at Transect 2 (Fig. 6) gives a freshwater discharge flux per meter coastline in the range of $1\text{--}4 \times 10^{-5} \text{ m}^3/\text{s m}$, but uncertainty increases since the flow-through area, the anisotropy as well as the hydraulic conductivity distribution are poorly constrained. In addition these flux estimates are highly affected by the tidal dynamics.

At the most detailed scale the flux of discharging freshwater can be measured by seepage meters (Fig. 7). The discharge pattern displayed in Fig. 7 reveal a large spatial variability of the SFGD even over a small stretch of coast. A similar variability in the discharge flux along a coastline has previously been reported by Valiela et al. (1990), Vanek and Lee (1991), Cable et al. (1997a) and Portnoy et al. (1998). Furthermore, for a specific discharge zone, the freshwater discharge fluxes appear to be highest close to the high tide line and then rapidly decline in the seaward direction as shown by Profiles 2 and 3 of Fig. 7. Similar patterns of seaward decreasing groundwater discharge have been found in other studies (Bokuniewicz, 1980, 1992; Lee, 1977; Cable et al., 1997a,b; Robinson et al., 1998).

The measured seepage rates are biased by the fact that seepage meter measurements can only be made when the seepage meters are submerged. It is therefore not possible to determine the discharge flux at low tide (Robinson et al., 1998) where the discharge flux may well be at maximum because the seaward hydraulic gradient is highest (Fig. 6). Furthermore the freshwater fluxes calculated using seepage meter discharge data may not be simply related to the pore water velocity when part of the discharging groundwater is brackish. However, the discharge measurements of Fig. 7 truthfully reveal the spatial variability of the SFGD over a small stretch of coast, since the three parallel transects were measured simultaneously using three seepage meters at equal distance from the high tide line and thus subject to the same conditions and potential errors.

Table 2 compares the different estimates of the freshwater discharge flux per meter coastline ($\text{m}^3/\text{m s}$), obtained at aquifer scale and at the local scale. The estimates based on the gradient method and the groundwater model for Location 1 are only weakly dependent, even though they are both based on the measured hydraulic conductivity in the coastal zone. This is because of the spatial distribution of recharge in the groundwater model; the distributed hydraulic conductivity; the distributed topography of the basal clay; and because the model is calibrated to produce the observed head gradients on the catchment scale. Furthermore, the freshwater discharge flux estimates obtained from the groundwater model reflect a steady state situation whereas both the estimates by the gradient method and the seepage meter estimates represent a transient situation. There is good correspondence between the discharge flux estimates by the different methods for locations 1 and 2

(Table 2). The largest discrepancy is observed for Location 1, where the model estimate of $1.7 \times 10^{-5} \text{ m}^3/\text{s m}$ is significantly higher than the estimate of $0.7 \times 10^{-5} \text{ m}^3/\text{s m}$ based on the gradient method. The low discharge estimate obtained by the gradient method can not be explained by a seasonally low discharge alone, since the transient groundwater model predicts a discharge that is only 9% lower than at steady state for a dry period (Fig. 10b). Rather the discrepancy could stem from the lack of head and hydraulic conductivity data at depths below 10 m in Transect 1. For the deeper zone (10–30 m) a hydraulic conductivity a factor 2–4 higher than the one used could easily explain the observed difference in the discharge flux. This would comply with the large freshwater zone seen in the lower part of the MEP 3 profile in Fig. 4.

The average integrated SFGD for the three seepage meter profiles in Fig. 7a gives an estimate that equals that of the steady state model output for this location (Table 2). This must be coincidental considering the local scale heterogeneities in the intertidal zone.

To summarize, discharge fluxes generated by the groundwater model are of more regional significance and best used to obtain the discharge per meter of shoreface. To be reliable it requires that the model contains the detailed geological structure at the shoreface. These models are less likely to produce good estimates for what is actually observed in the sub- and intertidal zones as for example measured by seepage meters.

The use of the gradient method to obtain groundwater fluxes relies on either a homogeneous geology or on closely spaced measurements of the hydraulic conductivity and may not be a suitable method for a complex coastal discharge zone (Lee, 1977; Giblin and Gaines, 1990; Tobias et al., 2001). It is also hampered by the transient flow conditions in the tidal zone as exemplified by Fig. 6.

The results obtained by seepage meters are apparently controlled by microheterogeneity. Mapping this microheterogeneity

may be important for understanding the behaviour of nutrients and pollutants in the coastal environment at a local scale.

Nitrate transport to the marine zone

The nitrate flux out through the shoreface is a product of the geological heterogeneity; the spatial and temporal application of fertilizers; the travel-time distribution in the aquifer; and finally the degradation of nitrate within the aquifer and sea-bottom.

The spatial distribution of the nitrate leaching from the root zone was calculated from the spatial fertilizer application over the 13 year period from 1989 to 2001, using DAISY-GIS and is shown in Fig. 11a. The mean annual nitrate flux to the groundwater varies spatially between 0–50 and 450 mmol/m^2 . Fig. 11a shows how especially the northeast quarter of the catchment is potentially affected by an agriculturally derived nitrate flux of up to 450 mmol/m^2 pr. year. With an average groundwater recharge rate of 396 mm/year this translates to a groundwater nitrate concentration of 1.1 mM . Measurements of the nitrate concentration in the shallow groundwater of the catchment (Fig. 1a) show reasonable agreement with the modeled soil leaching of nitrate (Fig. 11a) calculated by DAISY-GIS.

To elucidate the effect of travel time, particle tracking was simulated with the groundwater model run in a transient mode for more than 100 years using the calculated recharge for the period 1989–2001 in a cyclic mode. This 13-year period is sufficiently large to include the natural variation in recharge and therefore the particle tracking simulation will not be significantly influenced by the cyclic approach. Fig. 11b shows that groundwater recharged near the groundwater divide takes up to 100 years to reach the coastline and that groundwater recharged within the one quarter of the catchment area closest to the divide is about 20–60 years underway before reaching the discharge zone at the coastline.

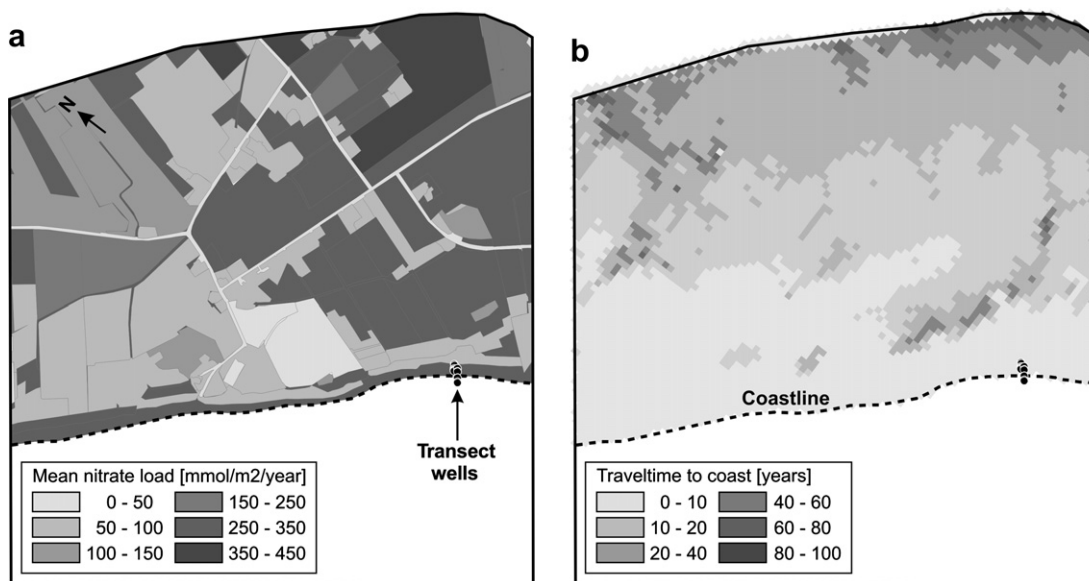


Figure 11 (a) Spatially distributed average yearly nitrate leakage from the root zone ($\text{mmol NO}_3^-/\text{m}^2 \text{ year}$) calculated by DAISY-GIS; (b) distribution of groundwater travel times to the coast in years based on particle tracking calculated by the steady state groundwater model. Notice that the plots are rotated relative to north.

However, for the transport of nitrate within the aquifer there is a lack of historical data on the temporal and spatial nitrate loading within the catchment prior to the 13 year period. But it is known on a national scale that there has been a steady increase in the usage of nitrate fertilizers up through the 1950s, 1960s and 1970s (Postma et al., 1991; Iversen et al., 1998). Because of this lack of detailed historical data we refrained from modeling the transport of nitrate through the aquifer.

In contrast to the nitrate contaminated shallow groundwater of the catchment (Figs. 1 and 11a) very little nitrate is found in the freshwater discharging through the shoreface into the marine environments. Generally along the coastline most of the nitrate detected in discharging groundwater has been found near the high tide line (Fig. 1) even though the zone of freshwater discharge extends much further into the intertidal zone. There are basically two possible (but not necessarily mutually exclusive) explanations for this. First it will depend on flow and transport of nitrate through the coastal aquifer. The intensive application of fertilizers, and thereby leaching of nitrate from the soil and into the aquifer started in Denmark in the late 1950s, increasing gradually until more or less stable concentrations around 1–2 mM NO₃ were attained around 1980 in young groundwater (Postma et al., 1991). Since the model estimated maximum groundwater travel time from the groundwater divide to the shoreline is up to 100 years (Fig. 11b), some of the fresh groundwater discharging at the shoreface should contain very little nitrate for purely historical reasons (Modica et al., 1998). According to the modeled travel-time distribution (Fig. 11b), groundwater recharged near the groundwater divide, predating the start of intensive nitrate application, should presently still be discharging at the coastline. Generally this groundwater would flow near the bottom of the aquifer and ideally discharge at the seaward extreme of the submarine discharge zone (Modica et al., 1998). Exceptionally high pore water resistivities were measured in the most seaward end of the fresh groundwater discharge zone (Fig. 5). At another site in Denmark, it was found that groundwater infiltrated before the start of intensive fertilization generally has a dissolved solids concentration that is about a factor two lower (Postma et al., 1991), and thus has a higher resistivity. This supports a scenario where the nitrate concentration is to some extent controlled by the historical load of nitrate leaching from the soil and the flow patterns through the aquifer. Comparable age distributions and patterns of transport have been observed for groundwater discharge to streams (Böhlke et al., 2002; Puckett et al., 2002) highlighting that the flux of groundwater nitrate towards surface water bodies is highly transient and complex.

However, part of the explanation for the low nitrate concentrations could be denitrification in the inland aquifer. Denitrification may occur in anoxic parts of aquifers, coupling nitrate reduction to the oxidation of pyrite or organic carbon (Appelo and Postma, 2005). This subject will be addressed in a subsequent paper.

Conclusions

The discharge of fresh groundwater from a coastal aquifer into the adjacent coastal marine environment is at our field site mainly controlled by large scale geological structures,

i.e. the sand filled buried channels that connect the aquifer with the shoreface sediment. The discharge zones at the shoreface vary strongly at a detailed scale along the coastline and must be related to small scale heterogeneity in the coastal sediments.

Geophysical methods like UMEP and MEP are powerful tools for mapping the distribution of freshwater saturated sediments at the shoreface and thereby identifying the zones of freshwater discharge. The discharge flux of freshwater from the aquifer into the marine environment may be derived at different scales. At the largest scale groundwater flow models probably produce the most reliable estimates for the freshwater discharge flux along the coastline. However, they can not reliably predict what may be observed at a small scale at the beach because the local heterogeneity is too large and because of interactions with the denser overlying seawater. For that purpose seepage meters and local hydraulic gradients are more useful. The seepage meter measurements indicate the highest discharge of freshwater near the high tide line and rapidly decreasing in a seaward direction. Reversely, due to the high variability, seepage meters are not practical for obtaining realistic discharge fluxes at a more regional scale.

Nitrate is abundant in the shallow groundwater of the coastal aquifer and is also present in the discharging groundwater at certain spots along the coast. However, on average very little nitrate is observed in the freshwater discharging at the coast. Part of the explanation is the historical development in the load of nitrate leached from the soil and into the aquifer. The other possible explanation for the low nitrate contents in the discharging groundwater is denitrification occurring in the aquifer. The long travel times of groundwater in the aquifer makes it difficult to relate current land-use and nitrate leaching from soils to the discharge of nitrate in the marine environment.

Acknowledgements

This research has been supported by the EC 5th Framework programme (FP5), contract no.: EVK3-CT-2001-00066. Thanks to Erik Rønn Lange, Ellen Zimmer Hansen and Lene Kirstejn Jensen, who supported in the field. Thanks to students: Jeppe R. Hansen, Christian S. Wittrup, Bianca Pedersen, Dani E.H. Mikkelsen, Ida Damgaard, Anne Gammeltoft, Mette Gram, Lisbeth Hansen and Mette Lundsbye for great cooperation in the field. Thanks to Torben Dolin for helping out with the final drafting. And thanks to the editor Colin Neal and the two anonymous reviewers for helpful comments.

Appendix A. Supplementary data

Supplementary data associated with this article can be found, in the online version, at [doi:10.1016/j.jhydrol.2006.12.023](https://doi.org/10.1016/j.jhydrol.2006.12.023).

References

- Abrahamsen, P., Hansen, S., 2000. Daisy: an open soil–crop–atmosphere system model. *Environ. Modell. Software* 15, 113–330.

- Andersen, M.S., 2001. Geochemical processes at a seawater–freshwater interface. Ph.D. Thesis, Technical University of Denmark, Kgs. Lyngby.
- Andersen, M.S., Nyvang, V., Jakobsen, R., Postma, D., 2005. Geochemical processes and solute transport at the seawater/freshwater interface of a sandy aquifer. *Geochim. Cosmochim. Acta* 69 (14), 3979–3994.
- Andersen, M.S., Jakobsen, R., Postma, D. (in preparation). Nitrate transport and reduction in a coastal aquifer.
- Appelo, C.A.J., Postma, D., 2005. *Geochemistry, Groundwater, and Pollution*, second ed. A.A. Balkema, Rotterdam, 649 pp.
- Arps, J.J., 1953. The effects of temperature on the density and electrical resistivity of sodium chloride solutions. *J. Pet. Technol. Tech. Note* 195, 17–20.
- Bai, W., 1989. Den geoelektriske metode. Report. Laboratoriet for Geoteknik, Ingeniørhøjskolen. Horsens Teknisk (in Danish).
- Böhlke, J.K., Wanty, R., Tuttle, M., Delin, G., Landon, M., 2002. Denitrification in the recharge area and discharge area of a transient agricultural nitrate plume in a glacial outwash sand aquifer, Minnesota. *Water Resour. Res.* 38 (7). doi:10.1029/2001WR00066.
- Bokuniewicz, H., 1980. Groundwater seepage into Great South Bay, New York. *Estuarine Coastal Sci.* 10, 437–444.
- Bokuniewicz, H., 1992. Analytical descriptions of subaqueous groundwater seepage. *Estuaries* 15 (4), 458–464.
- Bokuniewicz, H., 2001. Toward a coastal ground-water typology. *J. Sea Res.* 46, 99–108.
- Bokuniewicz, H., Buddemeier, R., Maxwell, B., Smith, C., 2003. The typological approach to submarine groundwater discharge (SGD). *Biogeochemistry* 66, 145–158.
- Brock, T.D., Lee, D.R., Janes, D., Winek, D., 1982. Groundwater seepage as a nutrient source to a drainage lake: Lake Mendota, Wisconsin. *Water Res.* 16, 1255–1263.
- Burnett, W.C., Chanton, J.P., Christoff, J.L., Kontar, E.A., Krupa, S.L., Lambert, M.J., Moore, W.S., O'Rourke, D., Paulsen, R.J., Smith, C.F., Smith, L., Taniguchi, M., 2002. Assessing methodologies for measuring groundwater discharge to the ocean. *EOS* 83 (11), 117–123.
- Burnett, W.C., Bokuniewicz, H., Huettel, M., Moore, W.S., Taniguchi, M., 2003. Groundwater and pore water inputs to the coastal zone. *Biogeochemistry* 66, 3–33.
- Cable, J.E., Burnett, W.C., Chanton, J.P., 1997a. Magnitude and variations of groundwater seepage along a Florida marine shoreline. *Biogeochemistry* 38, 189–205.
- Cable, J.E., Burnett, W.C., Chanton, J.P., Corbett, D.R., Cable, P.H., 1997b. Field evaluation of seepage meters in the coastal marine environment. *Estuarine Coastal Shelf Sci.* 45, 367–375.
- Cambareri, T.C., Eichner, E.M., 1997. Watershed delineation and ground water discharge to a coastal embayment. *Ground Water* 36 (4), 626–634.
- Capone, D.G., Bautista, M.F., 1985. A groundwater source of nitrate in nearshore marine sediments. *Nature* 313, 214–216.
- Conley, D.J., Kaas, H., Møhlenberg, F., Rasmussen, B., Windolf, J., 2000. Characteristics of Danish estuaries. *Estuaries* 23, 820–837.
- Corbett, D.R., Chanton, J.P., Burnett, W.C., Dillon, K., Rutkowski, C., Fourqurean, J.W., 1999. Patterns of groundwater discharge into Florida Bay. *Limnol. Oceanogr.* 44 (4), 1045–1055.
- Dahlin, T., 1996. 2D resistivity surveying for environmental and engineering applications. *First Break* 14 (7), 275–283.
- Danish Forest and Nature Agency, 1987. *Geofysik og råstofkortlægning*. Miljøministeriet, Skov- og Naturstyrelsen (in Danish).
- DHI, 2004. *DaisyGis User Manual*. DHI, Water and Environment, Hørsholm, Denmark.
- Duff, J.H., Toner, B., Jackman, A.P., Avanzino, R.J., Triska, F.J., 2000. Determination of groundwater discharge into a sand and gravel bottom river: a comparison of chloride dilution and seepage meter techniques. *Verh. Int. Verein. Limnol.* 27, 406–411.
- Giblin, A.E., Gaines, A.G., 1990. Nitrogen inputs to a marine embayment: the importance of groundwater. *Biogeochemistry* 10, 309–328.
- Graham, D.N., Butts, M.B., 2005. Flexible, integrated watershed modelling with MIKE SHE. In: Singh, V.P., Frevert, D.K. (Eds.), *Watershed Models*. CRC Press, ISBN 0849336090, pp. 245–272.
- Howarth, R.W., 1988. Nutrient limitation of net primary production in marine ecosystems. *Ann. Rev. Ecol.* 19, 89–110.
- Howarth, R.W., Billen, G., Swaney, D., Townsend, A., Jaworski, N., Lajtha, K., Downing, J.A., Elmgren, R., Caraco, N., Jordan, T., Berendse, F., Freney, J., Kudeyarov, V., Murdoch, P., Zhao-Liang, Z., 1996. Regional nitrogen budgets and riverine N & P fluxes for the drainages to the North Atlantic Ocean: natural and human influences. *Biogeochemistry* 35, 75–139.
- Hvorslev, J.M., 1951. Time lag and soil permeability in groundwater observations. Bulletin No. 36, 50 pp. US Corps of Engineer, Waterways Experiment Station, Vicksburg, MS.
- Iversen, T.M., Grant, R., Nielsen, K., 1998. Nitrogen enrichment of European inland and marine waters with special attention to Danish policy measures. *Environ. Pollut.* 102 (S1), 771–780.
- Jickells, T., 2005. External inputs as a contributor to eutrophication problems. *J. Sea Res.* 54, 58–69.
- Johannes, R.E., 1980. The ecological significance of the submarine discharge of groundwater. *Mar. Ecol. Prog. Ser.* 3, 365–373.
- Johannes, R.E., Hearn, C.J., 1985. The effect of submarine groundwater discharge on nutrient and salinity regimes in a coastal lagoon off Perth, Western Australia. *Estuarine Coastal Shelf Sci.* 21, 789–800.
- Kaleris, V., Lagas, G., Marczynek, S., Piotrowski, J.A., 2002. Modelling submarine groundwater discharge: an example from the western Baltic Sea. *J. Hydrol.* 265, 76–99.
- Krantz, D.E., Manheim, F.T., Bratton, J.F., Phelan, D.J., 2004. Hydrogeologic setting and ground water flow beneath a section of Indian River Bay, Delaware. *Ground Water* 42 (7), 1035–1051.
- Lagabriele, R., 1983. The effect of water on direct current resistivity measurement from the sea, river or lake floor. *Geoexploration* 21, 165–170.
- Lagabriele, R., Teilhaud, S., 1981. Prospection de gisements alluvionnaires de sites aquatiques par profils continus de résistivité au fond de l'eau. *Bull. Liaison Labo. P. et Ch.* 114, 17–24 (in French).
- Lapointe, B.E., O'Connell, J.D., Garrett, G.S., 1990. Nutrient couplings between on-site sewage disposal systems, groundwaters, and nearshore surface waters of the Florida Keys. *Biogeochemistry* 10, 289–307.
- Lee, D.R., 1977. A device for measuring seepage flux in lakes and estuaries. *Limnol. Oceanogr.* 22, 140–147.
- Lee, D.R., Cherry, J.A., 1978. A field exercise on groundwater flow using seepage meters and mini-piezometers. *J. Geol. Educ.* 25, 6–10.
- Lewis, J.B., 1987. Measurements of groundwater seepage flux onto a coral reef: spatial and temporal variations. *Limnol. Oceanogr.* 35 (2), 1162–1169.
- Libelo, E.L., MacIntyre, W.G., 1994. Effects of surface-water movement on seepage meter measurements of flow through the sediment–water interface. *Appl. Hydrogeol.* 4, 49–54.
- Loeb, S.L., Goldman, C.R., 1979. Water and nutrient transport via groundwater from Ward Valley into Lake Tahoe. *Limnol. Oceanogr.* 24 (6), 1146–1154.
- Loke, M.H., Barker, R.D., 1996. Rapid least-squares inversion of apparent resistivity pseudosections using a quasi-Newton method. *Geophysical Prospecting* 44, 131–152.
- Manheim, F.T., Krantz, D.E., Bratton, J.F., 2004. Studying ground water under Delmarva coastal bays using electrical resistivity. *Ground Water* 42 (7), 1052–1068.
- Matson, E.A., 1993. Nutrient flux through soils and aquifers to the coastal zone of Guam (Mariana Islands). *Limnol. Oceanogr.* 38 (2), 361–371.

- McMahon, P.B., Böhlke, J.K., 1996. Denitrification and mixing in a stream-aquifer system: effects on nitrate loadings to surface water. *J. Hydrol.* 186, 105–128.
- Mikkelsen, D.E.H., 2004. Geological and hydro-geological model for a beach aquifer (Sjælborg, Ho Bay). MSc. Thesis, Institute of Environment and Resources, The Technical University of Denmark, Kgs. Lyngby, p. 93.
- Modica, E., Buxton, H.T., Plummer, L.N., 1998. Evaluating the source and residence times of groundwater seepage to streams, New Jersey Coastal Plain. *Water Resour. Res.* 34 (11), 2797–2810.
- Moore, W.S., 1996. Large groundwater inputs to coastal waters revealed by ^{226}Ra enrichments. *Nature* 380, 612–614.
- Moore, W.S., 1999. The subterranean estuary: a reaction zone of ground water and sea water. *Mar. Chem.* 65, 111–125.
- Murdoch, L.C., Kelly, S.E., 2003. Factors affecting the performance of conventional seepage meters. *Water Resour. Res.* 39 (6). doi:10.1029/2002WR00134.
- Oberdorfer, J.A., Valentino, M.A., Smith, S.V., 1990. Groundwater contribution to the nutrient budget of Tomales Bay, California. *Biogeochemistry* 10, 199–216.
- Paerl, H.W., 1997. Coastal eutrophication and harmful algal blooms: importance of atmospheric deposition and groundwater as "new" nitrogen and other nutrient sources. *Limnol. Oceanogr.* 42 (5 part 2), 1154–1165.
- Portnoy, J.W., Nowicki, B.L., Roman, C.T., Urish, D.W., 1998. The discharge of nitrate-contaminated groundwater from developed shoreline to marsh-fringed estuary. *Water Resour. Res.* 34 (11), 3095–3104.
- Postma, D., Boesen, C., Kristiansen, H., Larsen, F., 1991. Nitrate reduction in an unconfined sandy aquifer: water chemistry, reduction processes, and geochemical modeling. *Water Resour. Res.* 27 (8), 2027–2045.
- Puckett, L.J., Cowdery, T.K., McMahon, P.B., Tornes, L.H., Stoner, J.D., 2002. Using chemical, hydrological and age dating analysis to delineate redox processes and flow paths in the riparian zone of a glacial outwash aquifer-stream system. *Water Resour. Res.* 38 (8). doi:10.1029/2001WR00039.
- Ribe County, 2003. Unpublished data. Ribe Amt, Natur- og grundvandsafdelingen, Amtsgården, Sorsigvej 35, 6760 Ribe, Denmark.
- Robinson, C., Gibbes, B., Li, L., 2006a. Driving mechanisms for groundwater flow and salt transport in a subterranean estuary. *Geophys. Res. Lett.* 33. doi:10.1029/2005GL02524.
- Robinson, C., Gibbes, B., Li, L., 2006b. Effect of tidal forcing on a subterranean estuary. *Adv. Water Resour.* doi:10.1016/j.advwatres.2006.07.006.
- Robinson, M.A., Gallagher, D.L., Reay, W.G., 1998. Field observations of tidal and seasonal variations in ground water discharge to tidal estuarine surface water. *Ground Water Monit. Remediat.* Winter 1998, 83–92.
- Rutkowski, C.M., Burnett, W.C., Iverson, R.L., Chanton, J.P., 1999. The effect of groundwater seepage on nutrient delivery and seagrass distribution in the Northeastern Gulf of Mexico. *Estuaries* 22 (4), 1033–1040.
- Ryther, J.H., Dunstan, W.M., 1971. Nitrogen, phosphorus, and eutrophication in coastal marine environments. *Science* 171 (3975), 1008–1013.
- Schlüter, M., Sauter, E.J., Andersen, C.E., Dahlgaard, H., Dando, P.R., 2004. Spatial distribution and budget for submarine groundwater discharge in Eckernförde Bay (Western Baltic Sea). *Limnol. Oceanogr.* 49, 157–167.
- Shinn, E.A., Reich, C.D., Hickey, T.D., 2002. Seepage meters and Bernoulli's revenge. *Estuaries* 25 (1), 126–132.
- Smith, A.J., Nield, S.P., 2003. Groundwater discharge from the superficial aquifer into Cockburn Sound Western Australia: estimation by inshore water balance. *Biogeochemistry* 66, 125–144.
- Smith, L., Zawadzki, W., 2003. A hydrogeologic model of submarine groundwater discharge: Florida intercomparison experiment. *Biogeochemistry* 66, 95–110.
- Spalding, R.F., Exner, M.E., 1993. Occurrence of nitrate in groundwater – a review. *J. Environ. Qual.* 22, 292–402.
- Slomp, C.P., Capellen, P.V., 2004. Nutrient inputs to the coastal ocean through submarine groundwater discharge: controls and potential impact. *J. Hydrol.* 295, 64–86.
- Staver, K.W., Brinsfield, R.B., 1996. Seepage of groundwater from a riparian agroecosystem into the Wye River Estuary. *Estuaries* 19 (2B), 359–370.
- Swarzenski, P.W., Reich, C.D., Spechler, R.M., Kindinger, J.L., Moore, W.S., 2001. Using multiple geochemical tracers to characterize the hydrogeology of the submarine spring off Crescent Beach, Florida. *Chem. Geol.* 179 (1–4), 187–202.
- Taniguchi, M., Iwakawa, H., 2004. Submarine groundwater discharge in Osaka Bay, Japan. *Limnology* 5, 25–32.
- Taniguchi, M., Burnett, W.C., Cable, J.E., Turner, J.V., 2002. Investigation of submarine groundwater discharge. *Hydrol. Process.* 16, 2115–2119.
- Taniguchi, M., Burnett, W.C., Smith, C.F., Paulsen, R.J., O'Rourke, D., Krupa, S.L., Christoff, J.L., 2003. Spatial and temporal distributions of submarine groundwater discharge rates obtained from various types of seepage meters at a site in the Northeastern Gulf of Mexico. *Biogeochemistry* 66, 35–53.
- Telford, W.M., Geldart, L.P., Sheriff, R.E., 1990. *Applied Geophysics*, second ed., Cambridge University Press, Cambridge.
- Tobias, C.R., Harvey, J.W., Anderson, I.C., 2001. Quantifying groundwater discharge through fringing wetlands to estuaries: seasonal variability, methods comparison, and implications for wetland–estuary exchange. *Limnol. Oceanogr.* 46 (3), 604–615.
- Tronicke, J., Blindow, N., Gross, R., Lange, M.A., 1999. Joint application of surface electrical resistivity- and GPR-measurements for groundwater exploration on the island of Spiekeroog – northern Germany. *J. Hydrol.* 223, 44–53.
- Turner, I.L., Acworth, R.I., 2004. Field measurements of beachface salinity structure using cross-borehole resistivity imaging. *J. Coastal Res.* 20 (3), 753–760.
- Urish, D.W., 1981. Electrical resistivity–hydraulic conductivity relationships in glacial outwash aquifers. *Water Resour. Res.* 17 (5), 1401–1408.
- Valiela, I., Teal, J.M., Volkmann, S., Shafer, D., Carpenter, E.J., 1978. Nutrient and particulate fluxes in a salt marsh ecosystem: tidal exchanges and inputs by precipitation and groundwater. *Limnol. Oceanogr.* 23 (4), 798–812.
- Valiela, I., Costa, J., Foreman, K., Teal, J.M., Howes, B., Aubrey, D., 1990. Transport of groundwater-borne nutrients from watersheds and their effects on coastal waters. *Biogeochemistry* 10, 177–197.
- Valiela, I., Foreman, K., LaMontagne, M., Hersh, D., Costa, J., Peckol, P., DeMeo-Anderson, B., D'Avanzo, C., Babione, M., Sham, C.-H., Brawley, J., Lajtha, K., 1992. Couplings of watersheds and coastal waters: sources and consequences of nutrient enrichment in Waquoit Bay, Massachusetts. *Estuaries* 15 (4), 443–457.
- Vandenbohede, A., Lebbe, L., 2006. Occurrence of salt water above fresh water in dynamic equilibrium in a coastal groundwater flow system near De Panne, Belgium. *J. Hydrogeol.* doi:10.1007/s10040-005-0446-5.
- Vanek, V., Lee, D.R., 1991. Mapping submarine groundwater discharge areas – an example from Laholm Bay, southwestern Sweden. *Limnol. Oceanogr.* 36 (6), 1250–1262.
- Worthington, A.E.P., Hedges, J.H., Pallatt, N., 1990. SCA guidelines for sample preparation and porosity measurement of electrical resistivity samples. Part I – guidelines for preparation of brine and determination of brine resistivity for use in electrical resistivity measurements. *Log Analyst* (January–February), 20–28.
- Zektzer, I.S., Ivanov, V.A., Meskheteli, A.V., 1973. The problem of direct groundwater discharge to the seas. *J. of Hydrol.* 20, 1–36.